7 The Constrained RPA Method for Calculating the Hubbard *U* from First-Principles

F. Aryasetiawan,[1] T. Miyake,[2,3] and R. Sakuma[1]

[1] Graduate School of Advanced Integration Science
Chiba University, Japan

[2] Nanosystem Research Institute, AIST, Japan

[3] Japan Science and Technology Agency, CREST

Contents

E. Pavarini, E. Koch, Dieter Vollhardt, and Alexander Lichtenstein
The LDA+DMFT approach to strongly correlated materials
Modeling and Simulation Vol. 1
Forschungszentrum Jülich, 2011, ISBN 978-3-89336-734-4
http://www.cond-mat.de/events/correl11

1 Introduction

Solving the many-electron problem is one of the main goals of condensed matter physics.Were it not for the presence of the Coulomb interaction among the electrons, the many-electron Hamiltonian could be easily solved since it amounts to solving a one-electron problem. The Hamiltonian without the Coulomb interaction is given by

$$H^0 = \sum_{n=1}^{N} h^0(r_n) = \sum_{n=1}^{N} \left[-\frac{1}{2}\nabla_n^2 + V_{\text{ext}}(r_n) \right] , \tag{1}$$

where we have worked in atomic units ($\hbar = m = e = 1 \rightarrow 1$ a.u.$= 27.2$ eV), $r_n = (\mathbf{r}_n, \sigma_n)$ is a combined variable for position and spin, and V_{ext} is an external potential, such as the potential from the nuclear charges. The problem becomes enormously complicated when the Coulomb interaction among the electrons is added to the above Hamiltonian:

$$H = H^0 + V \, , \tag{2}$$

where

$$V = \frac{1}{2}\sum_{i \neq j} v(r_i - r_j), \;\; v(r_i - r_j) = \frac{1}{|\mathbf{r}_i - \mathbf{r}_j|} \, . \tag{3}$$

Except for small systems, such as atoms and small molecules containing a few tens of electrons, there is little hope of solving the many-electron problem exactly, in particular for excited states, which are our main interest here. Various simplifications and techniques are needed in order to make progress.

In terms of field operators and in the occupation number representation the Hamiltonian takes the form [1]

$$\hat{H} = \int dr \hat{\psi}^+(r) \left[h^0(r) + \frac{1}{2}\hat{V}^{\text{H}}(r) \right] \hat{\psi}(r) \, , \tag{4}$$

where

$$\hat{V}^{\text{H}}(r) = \int dr' v(r - r') \hat{\psi}^+(r') \hat{\psi}(r') = \int dr' v(r - r') \hat{\rho}(r'). \tag{5}$$

We use the convention $\int dr = \sum_\sigma \int d^3r$. Since

$$\hat{\psi}(r) = \sum_n \varphi_n(r) c_n \, , \tag{6}$$

we obtain

$$\hat{H} = \sum_{ij} c_i^+ \left(h_{ij}^0 + \frac{1}{2}\hat{V}_{ij}^H \right) c_j \, , \tag{7}$$

where

$$\hat{V}_{ij}^H = \sum_{kl} v_{ij,kl} c_k^+ c_l, \tag{8}$$

and

$$h_{ij}^0 = \int dr \varphi_i^*(r) h^0(r) \varphi_j(r), \tag{9}$$

$$v_{ij,kl} = \int dr dr' \varphi_i^*(r)\varphi_j(r)v(r-r')\varphi_k^*(r')\varphi_l(r'). \tag{10}$$

The one-particle orbitals $\{\varphi_n\}$ are arbitrary but often chosen to be the Kohn-Sham orbitals. Note that the index n is a combined index of orbital and spin functions:

$$\varphi_n(r) = \varphi_k(\mathbf{r})\xi(\sigma),\ n = (k,\xi) \tag{11}$$

and that the definition of the Coulomb matrix is different from the usual convention. The definition in (10) is chosen to conform to the definition of the Hubbard U defined later.

A great simplification to the full many-electron Hamiltonian was introduced by Hubbard when studying the physics of transition metals in the late fifties. He noticed that most of the physics could well be attributed to electrons occupying the partially filled narrow $3d$ bands, which crossed the Fermi level. He then heuristically introduced the following Hamiltonian, now famously known as the Hubbard model [2]:

$$\hat{H} = \sum_{ij\subset 3d} c_i^+ h_{ij}^0 c_j + \frac{1}{2}\sum_{ijkl\subset 3d} U_{ij,kl} c_i^+ c_k^+ c_l c_j. \tag{12}$$

It is the same form as the Hamiltonian in (7) but the orbitals defining the annihilation and creation operators are now confined to the $3d$ orbitals and the Coulomb interaction has been replaced by some effective interaction U. The index i labels the atomic position and the localised $3d$ orbital. He reasoned that the rest of the electrons, that are more extended compared to the localised $3d$ electrons had the role of screening the Coulomb interaction between the $3d$ electrons and therefore the bare Coulomb interaction was reduced to an effective interaction U, the famous Hubbard U, which was assumed to have onsite components only, i.e., the labels i, j, k, l in $U_{ij,kl}$ refer to the same atomic site. Since then this seemingly simple looking model has had an enormous impact in the field of condensed matter physics as witnessed by a huge number of articles on works where the model has been used to study a wide range of problems from magnetism to superconductivity. The Hubbard model is suitable for studying materials with partially filled narrow bands. A large class of materials with this characteristic, often referred to as strongly correlated materials, are hosts to many intriguing physical properties [3] such as the metal-insulator transition and giant magnetoresistance. Small variations in the physical parameters, e.g., pressure or doping, can induce large changes in the physical properties.

Despite its simplicity the Hubbard model has proven to be highly non-trivial to solve, except for a few special cases such as the one-dimensional case. Even in its simplest form with only one orbital per site or one-band model,

$$\hat{H} = t\sum_{<i,j>} c_i^+ c_j + U\sum_i n_{i\uparrow} n_{i\downarrow}, \tag{13}$$

no exact solution is known. The notation $< ij >$ indicates that the hopping is restricted to the nearest neighbours only. In most cases the Hubbard model is then solved numerically by various methods. Among these we have the Lanczos method (exact diagonalisation), Quantum

Monte Carlo (QMC) method [4], and in recent years the dynamical mean-field theory (DMFT) method [5].

Central to the Hubbard model are the hopping parameters $t_{ij} = h^0_{ij}$ and the effective Coulomb interaction (Hubbard U) $U_{ij,kl}$. For the above simplest model there is actually only one effective parameter, namely, U/t. While it is relatively straightforward to extract the hopping parameters from realistic band structure calculations, it is much more elusive to determine the Hubbard U so that in many cases it is often treated as an adjustable parameter. To understand a generic physical phenomenon, it is quite appropriate to vary U in order to see the effects on the physical properties of interest. However, for a given material under a given condition, there does not seem to be any good reason to vary U since its value ought to be fixed. Different values of U simply correspond to different materials or different conditions. Reliable determination of U is therefore of utmost importance in order to be able to make quantitative predictions and to calculate materials properties from first principles. The present article is focused on the determination of the Hubbard U parameter from realistic first-principles calculations.

The problem of determining the Hubbard *U* from first principles has been addressed by a number of authors. One of the earliest works is the constrained local density approximation (cLDA) approach [6–8] where the Hubbard *U* is calculated from the total energy variation with respect to the occupation number of the localised orbital. A further improvement of this scheme was recently proposed [9]. Later, a different approach based on the random-phase approximation (RPA) was introduced [10, 11].

2 Screening and the random-phase approximation

In condensed matter physics, the concept of screening is crucial for understanding many of the physical properties of materials, especially metals. Take for example the famous anomaly associated with the disappearance of the density of states at the Fermi level in metals within the Hartree-Fock approximation, which neglects dynamic screening [12].

When a system of electrons is perturbed by a static external potential, the electrons will rearrange themselves in such a way as to minimize the total energy. If we introduce a positive test charge into the electronic system, the electrons will be attracted to surround the positive charge and in so doing reduce the total energy. The negative potential energy compensates for the increase in the kinetic energy due to the localisation of the electrons around the test charge. As a result of the electron accumulation around the test charge, the effective interaction between the test charge and an electron sufficiently outside the range where the electrons are accumulated becomes much weaker than the bare Coulomb interaction. In other words, the Coulomb interaction is screened. If the test charge is an electron, other electrons will be repelled and a screening hole is created which similarly screens the bare Coulomb interaction. In general, the perturbing field may be time dependent so that screening is a time-dependent or energy-dependent phenomenon. As a consequence, the screened interaction is retarded so that at finite frequencies it may become negative.

Consider applying a time-dependent perturbation $\delta\varphi$ to a system of electrons. The change in the

electron density induced by this perturbation generates in turn a change in the Hartree potential $\delta V_{\rm H}$ so that the total potential is given by

$$\delta V = \delta\varphi + \delta V_{\rm H}. \tag{14}$$

The induced Hartree potential $\delta V_{\rm H}$ screens the applied perturbation $\delta\varphi$ and the ratio between the screened and the applied field is defined to be the inverse dielectric function. To simplify the writing, we use the notation $1 = (r_1, t_1)$ keeping in mind that $r_1 = (\mathbf{r}_1, \sigma_1)$ as previously defined in the Introduction:

$$\begin{aligned}
\epsilon^{-1}(1,2) &= \frac{\delta V(1)}{\delta\varphi(2)} \\
&= \delta(1-2) + \frac{\delta V_{\rm H}(1)}{\delta\varphi(2)} \\
&= \delta(1-2) + \int d3v(1-3)\frac{\delta\rho(3)}{\delta\varphi(2)} \\
&= \delta(1-2) + \int d3v(1-3)R(3,2),
\end{aligned} \tag{15}$$

or in matrix notation

$$\epsilon^{-1} = 1 + vR. \tag{16}$$

The Coulomb potential $v(1-2)$ is given by

$$v(1-2) = v(|\mathbf{r}_1 - \mathbf{r}_2|)\delta(t_1 - t_2).$$

The δ-function indicates that the Coulomb interaction is instantaneous since we are dealing with non-relativistic cases. We have defined the linear density response function R according to

$$R(1,2) = \frac{\delta\rho(1)}{\delta\varphi(2)} \text{ or } \delta\rho(1) = \int d2R(1,2)\delta\varphi(2), \tag{17}$$

which describes a change in the electron density $\delta\rho$ induced by an arbitrary time-dependent perturbation $\delta\varphi$ to first order.
The Coulomb interaction $v(1-2)$ may be thought of as the Coulomb potential at point $\mathbf{r}_1$ arising from a unit point charge at position $\mathbf{r}_2$. If we regard this potential as a perturbation, according to (17), the change in the density due to this perturbation is given by,

$$\delta\rho(3,2) = \int d4R(3,4)v(4-2). \tag{18}$$

This induced charge generates in turn the Hartree potential

$$\delta V_{\rm H}(1,2) = \int d3v(1-3)\delta\rho(3,2), \tag{19}$$

which screens the Coulomb potential at point $\mathbf{r}_1$. The screened Coulomb potential at point $\mathbf{r}_1$ due to a unit point charge at point $\mathbf{r}_2$ is therefore given by

$$\begin{aligned} W(1,2) &= v(1-2) + \delta V_{\rm H}(1,2) \\ &= v(1-2) + \int d3\; v(1-3)\delta\rho(3,2) \\ &= v(1-2) + \int d3d4\; v(1-3)R(3,4)v(4-2) \\ &= \int d4\; \epsilon^{-1}(1,4)v(4-2). \end{aligned} \tag{20}$$

The last line is obtained from (15).

To describe formally the screening phenomenon, it is useful to work with the Green function in the interaction representation and employ the Schwinger functional derivative technique [13] as done by Hedin [14]. The Green function in the interaction or Dirac representation is defined as follows:

$$iG(1,2) = \frac{\left\langle \Psi_0 \left| T[\hat{S}\hat{\psi}_D(1)\hat{\psi}_D^+(2)] \right| \Psi_0 \right\rangle}{\left\langle \Psi_0 \left| \hat{S} \right| \Psi_0 \right\rangle} \tag{21}$$

where

$$\hat{S} = T\exp[-i\int d4\; \hat{\rho}(4)\varphi(4)]. \tag{22}$$

T is the time-ordering operator that puts the operators chronologically from right to left. The field operators are in the Dirac or interaction representation:

$$\hat{\psi}_D(\mathbf{r},t) = e^{i\hat{H}t}\hat{\psi}(\mathbf{r})e^{-i\hat{H}t}.$$

$\hat{H}$ is the Hamiltonian of the interacting electron system defined in (4) without the perturbing field φ. The state $|\Psi_0\rangle$ is the ground state of $\hat{H}$, i.e., it is the same as the Heisenberg ground state in the usual definition of the Green function [1]. As can be easily seen, the above definition of the Green function reduces to the usual definition in terms of the Heisenberg field operators when $\varphi = 0$. One of the merits of the interaction picture is that the field operators do not depend on the perturbing field φ. This property, as will be seen later, is very useful when taking the functional derivative of the Green function with respect to the perturbing field in order to calculate the linear density response function.

The Green function in (21) satisfies the equation of motion

$$\left(i\frac{\partial}{\partial t_1} - h(1)\right)G(1,2) - \int d3\; \Sigma(1,3)G(3,2) = \delta(1-2), \tag{23}$$

where Σ is the self-energy without the Hartree potential and

$$h = -\frac{1}{2}\nabla^2 + V_{\rm ext} + V_{\rm H} + \varphi.$$

Here, $V_{\rm ext}$ and $V_{\rm H}$ are respectively the external field, such as the field from the nuclei, and the Hartree field. By multiplying both sides of (23) from the right by the inverse of the Green function we obtain

$$G^{-1}(1,2) = \left(i\frac{\partial}{\partial t_1} - h(1) \right) \delta(1-2) - \Sigma(1,2). \tag{24}$$

Since $GG^{-1} = 1$ we also have in matrix notation the identity

$$\frac{\delta G}{\delta \varphi} G^{-1} + G \frac{\delta G^{-1}}{\delta \varphi} = 0 \rightarrow \frac{\delta G}{\delta \varphi} = -G \frac{\delta G^{-1}}{\delta \varphi} G. \tag{25}$$

We are now in the position to derive the equation for the linear response function or the screened Coulomb interaction. Since $\rho(1) = -iG(1,1^+)$, we find from (17)

$$\begin{aligned} R(1,2) &= \frac{\delta \rho(1)}{\delta \varphi(2)} \\ &= -i \frac{\delta G(1,1^+)}{\delta \varphi(2)} \\ &= i \int d3d4\, G(1,3) \frac{\delta G^{-1}(3,4)}{\delta \varphi(2)} G(4,1^+), \end{aligned} \tag{26}$$

where we have used the identity in (25). We now use the expression for the inverse of the Green function in (24) to calculate $\delta G^{-1}/\delta \varphi$:

$$\frac{\delta G^{-1}(3,4)}{\delta \varphi(2)} = -\left[\delta(3-2) + \frac{\delta V_{\rm H}(3)}{\delta \varphi(2)} \right] \delta(3-4) - \frac{\delta \Sigma(3,4)}{\delta \varphi(2)}. \tag{27}$$

The first term on the right-hand side arises from $\delta\varphi(3)/\delta\varphi(2) = \delta(3-2)$. At this stage we will only keep the change in the Hartree potential and drop the term $\delta\Sigma/\delta\varphi$. This corresponds to the RPA, which may be regarded as the time-dependent Hartree approximation, since we only consider the change in the Hartree potential upon application of a time-dependent perturbation:

$$\frac{\delta V_{\rm H}(3)}{\delta \varphi(2)} = \frac{\delta}{\delta \varphi(2)} \int d5\, v(3-5) \rho(5) = \int d5\, v(3-5) R(5,2), \tag{28}$$

Within the RPA we then have

$$\frac{\delta G^{-1}(3,4)}{\delta \varphi(2)} = -\left[\delta(3-2) + \int d5\, v(3-5) R(5,2) \right] \delta(3-4). \tag{29}$$

Using this in (26) we arrive at

$$\begin{aligned} R(1,2) &= -i \int d3\, G(1,3) \left[\delta(3-2) + \int d5\, v(3-5) R(5,2) \right] G(3,1^+) \\ &= P(1,2) + \int d3d5\, P(1,3) v(3-5) R(5,2), \end{aligned} \tag{30}$$

where we have defined the polarisation function

$$P(1,2) = -iG(1,2)G(2,1^+). \tag{31}$$

In matrix form

$$R = P + PvR \rightarrow R = [1 - Pv]^{-1} P, \tag{32}$$

which is the well-known RPA equation. We note that, while in the RPA the polarisation function P is approximated by (31), the exact response function R satisfies the same equation with the exact polarization function P. It is straightforward to verify using (16) and (32) that the dielectric function is given by

$$\epsilon = 1 - vP \ : \tag{33}$$

$$\begin{aligned} \epsilon\epsilon^{-1} &= (1 - vP)(1 + vR) \\ &= 1 + vR - v(P + PvR) \\ &= 1. \end{aligned} \tag{34}$$

Using the convolution theorem, the Fourier transform of P in (31) is given by

$$P(r, r'; \omega) = -i \int \frac{d\omega}{2\pi} G(r, r'; \omega + \omega') G(r', r; \omega') \, , \tag{35}$$

where the Fourier transform is defined according to

$$G(\omega) = \int dt \; e^{i\omega t} G(t), \quad G(t) = \int \frac{d\omega}{2\pi} \; e^{-i\omega t} G(\omega) \, .$$

Using a non-interacting Green function

$$G^0(r, r'; \omega) = \sum_n^{\text{occ}} \frac{\varphi_n(r)\varphi_n^*(r')}{\omega - \varepsilon_n - i\delta} + \sum_m^{\text{unocc}} \frac{\varphi_m(r)\varphi_m^*(r')}{\omega - \varepsilon_m + i\delta} \, , \tag{36}$$

where $\{\varphi_n, \varepsilon_n\}$ are usually taken to be the Kohn-Sham orbitals and eigenvalues, the frequency integral can be performed analytically using Cauchy's theorem. Terms involving products of two occupied states or two unoccupied states vanish because the two poles lie on the same plane. Only terms involving the products of occupied and unoccupied states survive. For example, considering only the frequency-dependent parts,

$$-i \int \frac{d\omega}{2\pi} \left(\frac{1}{\omega + \omega' - \varepsilon_n - i\delta} \right)_{\text{occ}} \times \left(\frac{1}{\omega' - \varepsilon_m + i\delta} \right)_{\text{unocc}}$$

can be integrated analytically using the Cauchy theorem by closing the contour along an infinitely large semicircle either in the upper or lower half plane. This yields

$$\frac{-i}{2\pi}(2\pi i \times \text{residue}) = -\frac{1}{\omega + \varepsilon_m - \varepsilon_n - i\delta}.$$

Consequently,

$$\begin{aligned} P(r, r'; \omega) &= -\sum_n^{\text{occ}} \sum_m^{\text{unocc}} \frac{\varphi_n(r)\varphi_n^*(r')\varphi_m(r')\varphi_m^*(r)}{\omega + \varepsilon_m - \varepsilon_n - i\delta} \\ &\quad + \sum_n^{\text{occ}} \sum_m^{\text{unocc}} \frac{\varphi_n(r')\varphi_n^*(r)\varphi_m(r)\varphi_m^*(r')}{\omega - \varepsilon_m + \varepsilon_n + i\delta}, \end{aligned} \tag{37}$$

which can be rewritten more compactly as a sum over occupied and unoccupied pairs of orbitals

$$P(r, r'; \omega) = \sum_\alpha \left(\frac{b_\alpha(r) b_\alpha^*(r')}{\omega - \Delta_\alpha + i\delta} - \frac{b_\alpha^*(r) b_\alpha(r')}{\omega + \Delta_\alpha - i\delta} \right) , \tag{38}$$

where

$$b_\alpha = \varphi_n^* \varphi_m, \quad \Delta_\alpha = \varepsilon_m - \varepsilon_n > 0. \tag{39}$$

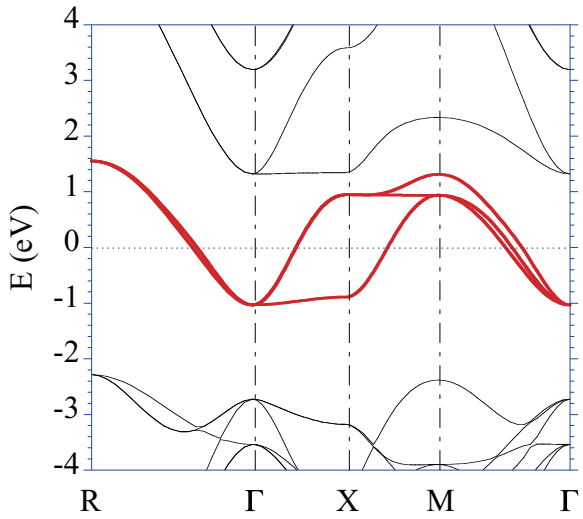

Fig. 1: *The band structure of $SrVO_3$. The red bands correspond to the vanadium 3d orbitals of t_{2g} character. Although the density of states corresponding to the red bands overlap with the rest of the density of states, as can be seen in Fig. 2, the red bands originating from the vanadium 3d t_{2g} orbitals are isolated from the rest of the bands.*

3 Constrained RPA

3.1 Theory

Let us consider a system with a narrow band, well separated from other bands, crossing the Fermi level. As a concrete example, consider the case of the perovskite $SrVO_3$, whose band structure and density of states are shown in Figs. 1 and 2. We first divide the one-particle Hilbert space into two parts, which we call the d and r subspaces. The d subspace is identified with the narrow band, which in the example of $SrVO_3$ are marked in red.
We may separate the total polarisation of the system into the polarisation within the d subspace, which we shall call P_d, and the rest of the polarisation, which we shall call P_r:

$$P = P_d + P_r. \tag{40}$$

The meaning of P_d and P_r is illustrated in Fig. 3. In the example of $SrVO_3$, the red bands in Fig. 1 form our d subspace, which corresponds to the subspace of our model and we wish to determine the Hubbard U or the effective interaction among electrons residing in the red bands. From (20) the fully screened Coulomb interaction is given by

$$W = \epsilon^{-1} v, \tag{41}$$

where from (16) and (33)

$$\epsilon^{-1} = 1 + vR \text{ and } \epsilon = 1 - vP. \tag{42}$$

The fully screened interaction can be rewritten as

$$W = [1 - W_r P_d]^{-1} W_r, \tag{43}$$

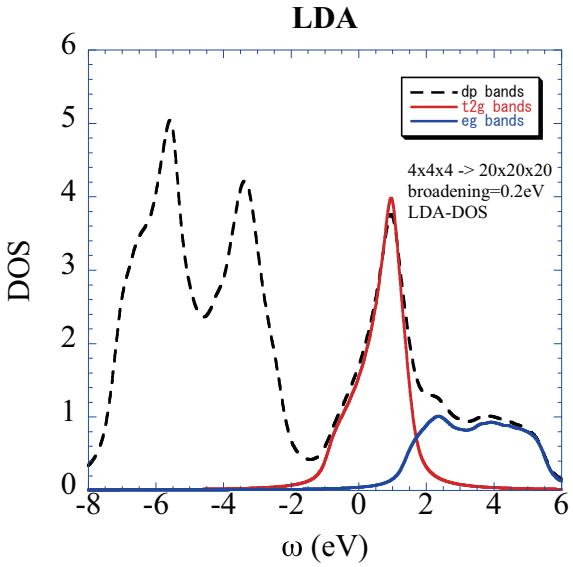

Fig. 2: *Density of states of $SrVO_3$. The dotted curve is the total density of states. The red and blue curves show the vanadium $3d$ t_{2g} and e_g components, respectively. The density of states between -8 to -2 eV originates from the oxygen $2p$ states.*

where

$$W_r = [1 - vP_r]^{-1}v = \epsilon_r^{-1}v. \tag{44}$$

We verify the above identity. From (41) and (42)

$$\begin{aligned} W &= [1 - vP]^{-1}v \\ &= [1 - vP_r - vP_d]^{-1}v \\ &= \left\{\epsilon_r[1 - \epsilon_r^{-1}vP_d]\right\}^{-1} v \\ &= [1 - \epsilon_r^{-1}vP_d]^{-1}\epsilon_r^{-1}v \\ &= [1 - W_rP_d]^{-1}W_r. \end{aligned} \tag{45}$$

We observe that the identity in Eq. (43) allows us to interpret W_r as the effective interaction among electrons residing in the d subspace or the Hubbard U [15] because when this effective interaction is screened further in the model by P_d we obtain the fully screened interaction:

$$U(\mathbf{r}, \mathbf{r}'; \omega) = W_r(\mathbf{r}, \mathbf{r}'; \omega). \tag{46}$$

A formal derivation of the Hubbard U from the many-electron Hamiltonian may be found in [16]. The Hubbard U is frequency dependent as a consequence of retarded screening effects.

Eq. (44) is exact, but in practice we approximate $P_r = P - P_d$ within the RPA, which takes the form

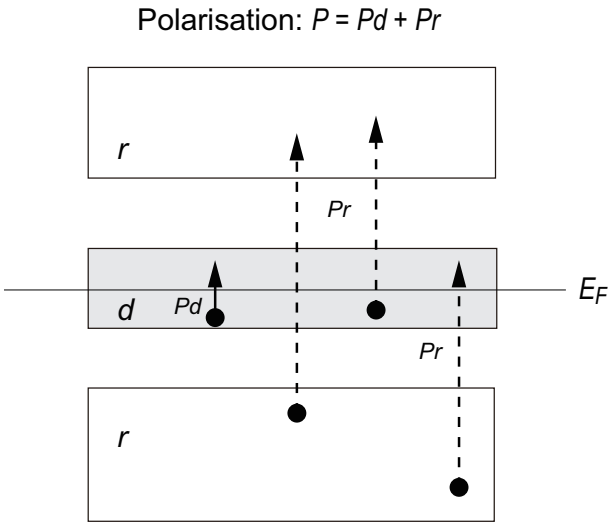

Fig. 3: *A schematic picture explaining the meaning of P_d and P_r. While P_d is confined to the transitions within the d subspace, P_r may contain transitions between the d and r subspaces.*

$$P(\mathbf{r},\mathbf{r}';\omega) = \sum_{kn}^{\text{occ}}\sum_{k'n'}^{\text{unocc}} \left\{ \frac{\psi^*_{kn}(\mathbf{r})\psi_{k'n'}(\mathbf{r})\psi^*_{k'n'}(\mathbf{r}')\psi_{kn}(\mathbf{r}')}{\omega - \varepsilon_{k'n'} + \varepsilon_{kn} + i\delta} - \frac{\psi_{kn}(\mathbf{r})\psi^*_{k'n'}(\mathbf{r})\psi_{k'n'}(\mathbf{r}')\psi^*_{kn}(\mathbf{r}')}{\omega + \varepsilon_{k'n'} - \varepsilon_{kn} - i\delta} \right\}, \tag{47}$$

where $\{\psi_{kn}, \varepsilon_{kn}\}$ are usually chosen to be the Kohn-Sham eigenfunctions and eigenvalues and $k = (\mathbf{k}, \sigma)$ is a combined index for the $\mathbf{k}$-vector and the spin σ. For systems without spin-flipping processes, k and k' evidently have the same spin. P_d has exactly the same form as in Eq. (47) but with the bands n and n' restricted to the d subspace. We note that P_r contains not only transitions inside the r subspace but also transitions between the d and r subspaces as illustrated in Fig. 3.

Since P_r does not contain low-energy polarisations that are responsible for metallic screening, U becomes long range. The asymptotic decay of U as a function of distance is expected to behave according to $1/(\alpha r)$ where $\alpha > 1$ rather than exponential, as often assumed. This behaviour is illustrated, e.g., in the case of the BEDT-TTF organic conductors [17].

It may be argued that for narrow-band materials with strong correlations it would not be sufficient to calculate U within the RPA. We would like to point out that from a physical point of view much of the error in the RPA resides in P_d rather than P_r because the former corresponds to the polarisation of the narrow bands, where we expect vertex corrections to the RPA to be large, whereas the latter corresponds to polarisation involving more extended states, for which the RPA is supposed to perform well. Since it is P_r that enters into the calculation of U, we expect that the error in the RPA has much less influence on U than one would anticipate.

In practice, Eq. (44) is solved by introducing a set of basis functions, and the choice of basis functions depends on the band-structure method. For band-structure methods based on pseudopotentials, a plane-wave basis set is a natural choice. For band-structure methods based on

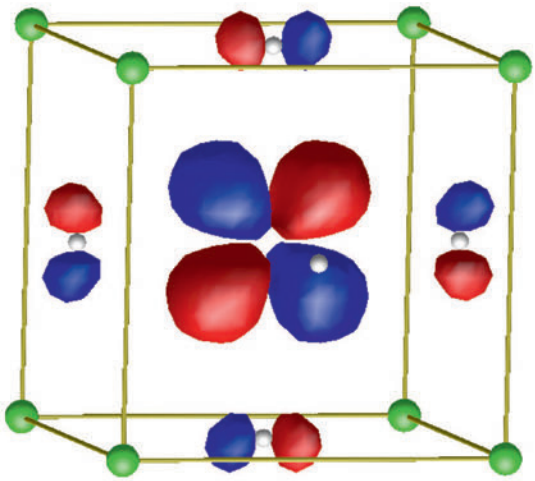

Fig. 4: *Contour plot of the maximally localized Wannier function (MLWF) of $SrVO_3$. If we take the x axis to be the horizontal direction and the z axis to be the vertical direction, the Wannier function corresponds to xz. The red (blue) represents the positive (negative) contour. The Wannier function is centered at the vanadium site, which is located at the center of the cube. The green spheres at the corners are strontium atoms, and white spheres at the centers of the faces are oxygen atoms. The MLWF is optimized in the t_{2g} model which consists of three t_{2g}-like states. We note that the Wannier function has tails on the oxygen sites.*

localised basis functions, such as the linear muffin-tin orbital (LMTO) method, the linearised augmented plane-wave method (LAPW) [18], or the Korringa-Kohn-Rostocker (KKR) method, a product basis set [19, 20] is usually used. This is described in the Appendix.

3.2 Wannier orbitals

After obtaining $U(\mathbf{r}, \mathbf{r}'; \omega)$ the next step is to calculate its matrix elements in some localised orbitals. The Hubbard model in Eq. (12) is defined with respect to a chosen one-particle basis set defining the creation and annihilation operators of the field operators. We must therefore calculate the matrix elements of U in this chosen one-particle basis set. It is of course up to us what basis we choose but an appealing choice is the maximally localised Wannier orbitals which are constructed as follows [21].

The Wannier function with band index n at cell $\mathbf{R}$ is defined by

$$|\varphi_{n\mathbf{R}}\rangle = \frac{V}{(2\pi)^3}\int d^3k\, e^{-i\mathbf{k}\cdot\mathbf{R}}|\psi^{(\mathrm{w})}_{\mathbf{k}n}\rangle, \tag{48}$$

where $|\psi^{(\mathrm{w})}_{\mathbf{k}n}\rangle$ is the associated Bloch function, which can be expanded as a linear combination of the eigenfunctions of a mean-field Hamiltonian as

$$|\psi^{(\mathrm{w})}_{\mathbf{k}n}\rangle = \sum_m |\psi_{\mathbf{k}m}\rangle \mathcal{U}_{mn}(\mathbf{k}). \tag{49}$$

In practical implementations, the Kohn-Sham wavefunctions are usually used for $|\psi_{\mathbf{k}m}\rangle$. In the maximally localised Wannier function scheme, the coefficients $\mathcal{U}_{mn}(\mathbf{k})$ are determined such

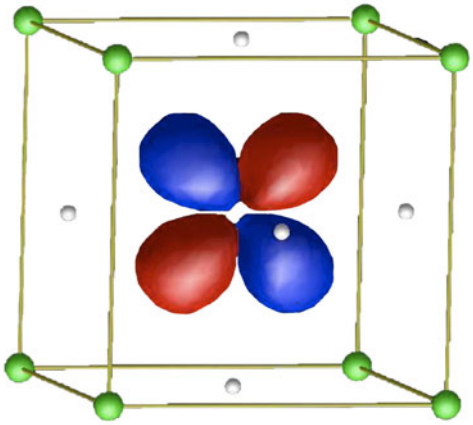

Fig. 5: *As in Fig. 4 but the Wannier function is constructed according to the dp model which consists of the vanadium $3d$ bands (t_{2g}+e_g) and oxygen $2p$ bands. Compared to the one in Fig. 4 the Wannier function has become much more localised on the vanadium site.*

that the quadratic extent of the wavefunctions

$$\Omega = \sum_n (\langle \varphi_{n\mathbf{0}} | r^2 | \varphi_{n\mathbf{0}} \rangle - |\langle \varphi_{n\mathbf{0}} | \mathbf{r} | \varphi_{n\mathbf{0}} \rangle|^2) \tag{50}$$

is minimised. When the bands are isolated, the Wannier orbitals are well defined and span the same Hilbert space as that of the isolated bands. However, when the bands are not isolated the Wannier orbitals are not unique. For this case, we introduce an energy window and optimise $\mathcal{U}_{mn}(\mathbf{k})$ with m limited to the states inside the window. The Wannier function is the more localised the larger the energy window, since optimisation is then done in a wider Hilbert space. This is illustrated in Figs. 4 and 5.

3.3 cRPA with the maximally localised Wannier function

Once $\mathcal{U}_{mn}(\mathbf{k})$ is determined on a k mesh, maximally localised Wannier functions are obtained by Fourier transform as in (48), from which the Hamiltonian corresponding to the d subspace is constructed: $H_{mn}(\mathbf{R}) = \langle \varphi_{m\mathbf{0}} | H | \varphi_{n\mathbf{R}} \rangle$. By Fourier transforming $H_{mn}(\mathbf{R})$ back to k space and diagonalising it, we reproduce the original narrow bands. If the narrow bands forming the d subspace are not completely separated from the rest of the bands, the resulting bands will no longer in general be the same as the original bands. For the case of $SrVO_3$ we first construct from the red bands in Fig. 1 three Wannier orbitals having strong $3d$ character of t_{2g} symmetry. The next step is to compute the screened Coulomb interaction $W_r(\mathbf{r}, \mathbf{r}'; \omega)$ in the cRPA and take the matrix elements in the maximally localised Wannier basis [22]:

$$W_r(n_1, n_2, n_3, n_4; \mathbf{R}; \omega) \equiv \int\int d^3r d^3r' \varphi^*_{n_1\mathbf{0}}(\mathbf{r}) \varphi_{n_2\mathbf{0}}(\mathbf{r}) W_r(\mathbf{r}, \mathbf{r}'; \omega) \varphi^*_{n_3\mathbf{R}}(\mathbf{r}') \varphi_{n_4\mathbf{R}}(\mathbf{r}'). \tag{51}$$

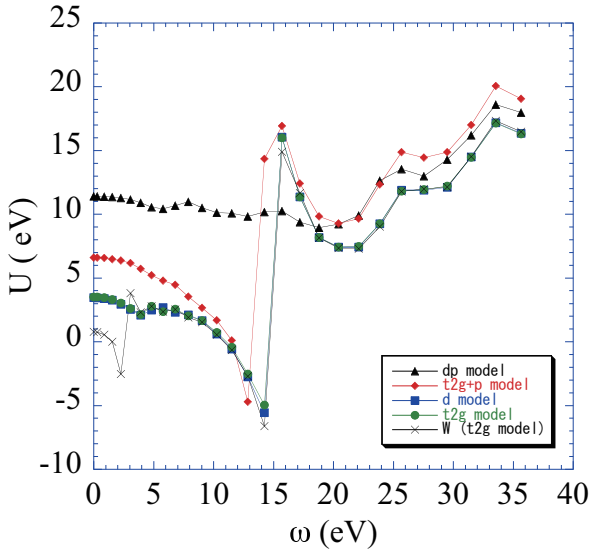

Fig. 6: *The real part of the Hubbard U for various d subspaces indicated by the legends in the figure. W is the fully screened interaction. The meaning of the legends is summarised in the table below. For example, the d subspace of the $t_{2g}+p$ model is comprised of the vanadium t_{2g} and oxygen p bands.*

model:	t_{2g}	d	$t_{2g}+p$	dp
d subspace:	$V\,t_{2g}$	$V\,(t_{2g}+e_g)$	$V\,t_{2g}+O\,p$	$V\,(t_{2g}+e_g)+O\,p$

The above expression is the most general, but in practice we often restrict ourselves to the on-site values and only consider the direct (charge-charge) and exchange components. The on-site Hubbard U matrix is defined to be

$$U_{nm}(\omega) \equiv \int\int d^3r d^3r' |\varphi_{n\mathbf{0}}(\mathbf{r})|^2 W_r(\mathbf{r},\mathbf{r}';\omega)|\varphi_{m\mathbf{0}}(\mathbf{r}')|^2 \tag{52}$$

and the onsite exchange matrix J.

$$J_{nm}(\omega) \equiv \int\int d^3r d^3r' \varphi^*_{n\mathbf{0}}(\mathbf{r})\varphi_{m\mathbf{0}}(\mathbf{r}) W_r(\mathbf{r},\mathbf{r}';\omega)\varphi_{n\mathbf{0}}(\mathbf{r}')\varphi^*_{m\mathbf{0}}(\mathbf{r}'). \tag{53}$$

Note that the definitions of U and J may vary according to convention but in any case the various definitions can be related to (52) and (53). At this point it is worth pointing out that the effective screened interaction $W_r(\mathbf{r},\mathbf{r}';\omega)$ calculated using the cRPA method is completely independent of the choice of basis functions. The *matrix elements* are of course dependent on the choice of the orbitals $\{\varphi_{n\mathbf{0}}\}$.

3.4 Example: $SrVO_3$

To illustrate the usefulness of the cRPA method in studying the screening properties of materials, we consider for $SrVO_3$ the calculations of U for various models. Although we have illustrated the cRPA scheme for a narrow band, the choice of the d subspace is entirely arbitrary and it may not necessarily correspond to a narrow band.

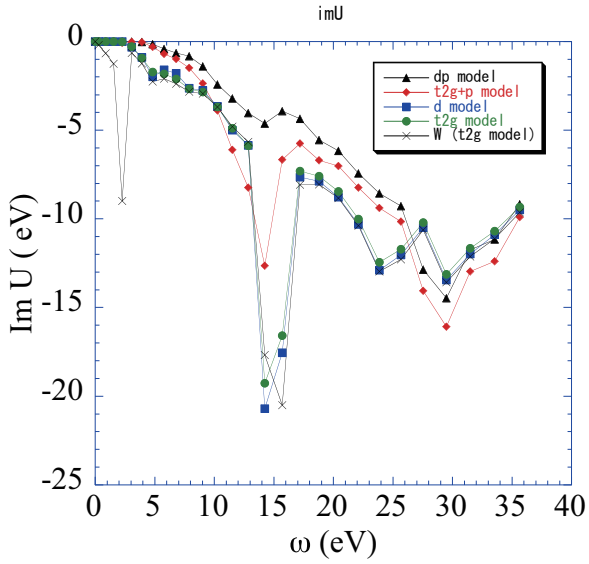

Fig. 7: *The imaginary part of the Hubbard U for the models indicated by the legends in the picture. W is the fully screened interaction. For the definitions of the models, see the caption of Fig. 6.*

We consider first the fully screened interaction W. Two notable features are clearly discernible in Fig. 7: there is the usual high-energy electron-gas-like plasmon excitation at around 16 eV and more remarkably there is a strong excitation between $2 \sim 3$ eV, which arises mainly from the collective excitation within the partially filled t_{2g} bands. That this is indeed the case can be understood by comparison with $U(\omega)$ for the t_{2g} model in Figs. 7 and 6, where the d subspace is formed by the t_{2g} bands. The structure at $2 \sim 3$ eV is almost absent, due to the elimination of the polarisation within the t_{2g} bands when calculating $U(\omega)$.

Comparison between the t_{2g}- and the d model, where both the t_{2g} and the e_g bands form the d subspace, clearly shows that the corresponding Hubbard U's are almost the same implying that the $t_{2g} \rightarrow e_g$ screening channel is essentially ineffective as can be seen in Fig. 6.

When the t_{2g} model is enlarged to the $t_{2g} + p$ model, where the d subspace is formed by the vanadium t_{2g} and the oxygen $2p$ bands, the corresponding static Hubbard U is almost doubled from 3.5 eV to 6.5 eV as shown in Fig. 6, demonstrating the important role of the oxygen p electrons in screening the Coulomb interaction. When calculating U in the $t_{2g} + p$ model, the $O_p \rightarrow t_{2g}$ screening channel is left out, and it is the elimination of this screening channel that is responsible for the large increase in the low-energy U. Furthermore, since the amount of screening channels is reduced compared with that of the t_{2g} only model, the onset of the plasmon excitation at around 16 eV is lowered by about 2 eV. In other words, the effective number of electron participating in the formation of plasmon excitations is reduced. It is noteworthy that the onset of the plasmon excitation in the t_{2g} and d models is unchanged, indicating that the plasmon excitation is not coupled to the polarisation within the d bands.

In the most expanded dp model, where the d subspace consists of the vanadium t_{2g} and e_g and the oxygen $2p$ bands, the value of the static U is approximately doubled further to 11 eV as can

be seen in Fig. 6, due to the elimination of the $O_p \rightarrow e_g$ screening, giving further evidence for the importance of the oxygen p electrons in the screening process. It can also be seen that the plasmon onset almost disappears, showing that the plasmon excitation mainly couples to the oxygen p electrons.

3.5 cRPA for entangled bands

Although the cRPA method is rather general, a serious technical problem arises when the narrow band is entangled with other bands, i.e., the narrow band is not completely isolated from the rest of the bands, a situation which occurs in many materials. For example, in $3d$ transition metals, the $3d$ bands mix with the $4s$ and $4p$ bands as illustrated in Fig. 8 and similarly the $4f$ bands of the $4f$ metals hybridise with the more extended $6s$ band. For such cases, it is not obvious anymore how to determine P_r in order to calculate U using the cRPA method.

A number of procedures have been proposed to handle the problem of determining U for entangled bands. One proposal is to choose a set of band indices and define the corresponding bands as the one-particle bands in the Hubbard model. Another proposal is to introduce an energy window and define the one-particle bands to be those that have energies within the energy window. Yet another proposal is to have a combination of energy window and band indices. These procedures, however, suffer from a number of difficulties. When choosing band indices it is likely that some of the states will have a character very different from that of the intended model. For example, in the case of the $3d$ transition metals, choosing five "$3d$" bands will include at some $\mathbf{k}$-points states which contains a considerable $4s$ component but little $3d$ character. Moreover, the chosen bands will not in general form smoothly connected bands. A similar problem is encountered when choosing an energy window. A hybrid construction using band indices and energy window [23] removes part of the problem but it is somewhat arbitrary. Another procedure is, as we will discuss in detail later, to project the polarisation to the orbitals of interest, e.g., $3d$ orbitals, but this procedure has been found to yield an unphysical result of negative static U.

To overcome the problem with entangled bands we propose the following procedure. We first construct a set of localised Wannier orbitals from a given set of bands defined within a certain energy window by following the post-processing procedure of Souza, Marzari and Vanderbilt [21] or other methods, such as the preprocessing scheme proposed by Andersen *et al.* within the Nth-order muffin-tin orbital (NMTO) method [24]. We then choose this set of Wannier orbitals as the d subspace and use them as a basis for diagonalising the one-particle Hamiltonian, which is usually the Kohn-Sham Hamiltonian in the local density approximation (LDA) or generalised gradient approximation (GGA). The so obtained set of bands, which equivalently define the d subspace, may be slightly different from the original bands defined within the chosen energy window. It is therefore important to confirm that the dispersions near the Fermi level well reproduces the original Kohn-Sham bands. From these bands we calculate the polarisation $\tilde{P}_d$,

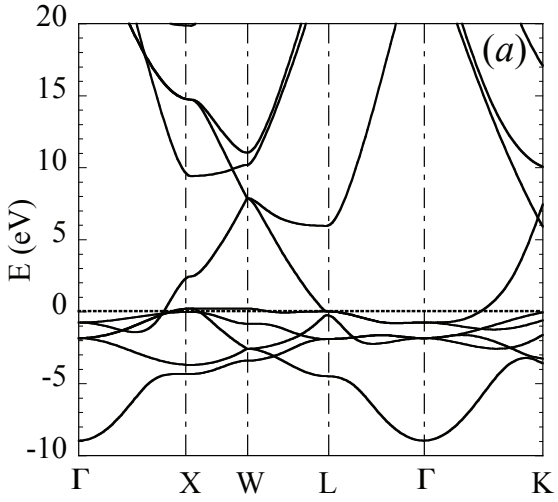

Fig. 8: *The band structure of paramagnetic nickel taken from [25]. The* $3d$ *band is approximately between* -4 *eV and slightly above the Fermi level (zero energy).*

$$\tilde{P}_d(\mathbf{r},\mathbf{r}';\omega) = \sum_i^{\text{occ}} \sum_j^{\text{unocc}} \left[\frac{\tilde{\psi}_i^*(\mathbf{r})\tilde{\psi}_j(\mathbf{r})\tilde{\psi}_j^*(\mathbf{r}')\tilde{\psi}_i(\mathbf{r}')}{\omega - \tilde{\varepsilon}_j + \tilde{\varepsilon}_i + i\delta} - \frac{\tilde{\psi}_i(\mathbf{r})\tilde{\psi}_j^*(\mathbf{r})\tilde{\psi}_j(\mathbf{r}')\tilde{\psi}_i^*(\mathbf{r}')}{\omega + \tilde{\varepsilon}_j - \tilde{\varepsilon}_i - i\delta} \right] , \tag{54}$$

where $\{\tilde{\psi}_i\}$, $\{\tilde{\varepsilon}_i\}$ $(i = 1, \ldots N_d)$ are the wavefunctions and eigenvalues obtained from diagonalising the one-particle Hamiltonian in the Wannier basis.
It would seem sensible to define the rest of the polarisation as $P_r = P - \tilde{P}_d$, where P is the full polarisation calculated using the *original* (Kohn-Sham) wavefunctions and eigenvalues $\{\psi_i\}$, $\{\varepsilon_i\}$ $(i = 1, \ldots N)$, and calculate W_r according to Eq. (44). We have found, however, that this procedure is numerically very unstable, resulting in some cases in unphysical negative static U and large oscillations at low energy. The reason is that $\tilde{P}_d$ does not completely encompass the low-energy excitations so that low energy screening channels associated with the d-d transitions are not completely excluded from P_r. Due to the singular nature of the expression in Eq. (44) these remaining low-energy excitations can cause large fluctuations in W_r.
Another way of calculating P_r is to project the wavefunctions to the d space,

$$|\bar{\psi}_i\rangle = \hat{\mathcal{P}}|\psi_i\rangle \ , \tag{55}$$

where the projection operator $\hat{\mathcal{P}}$ is defined as

$$\hat{\mathcal{P}} = \sum_{j=1}^{N_d} |\tilde{\psi}_j\rangle\langle\tilde{\psi}_j| \ . \tag{56}$$

The effective d polarisation may be expressed as

$$\bar{P}_d(\mathbf{r},\mathbf{r}';\omega) = \sum_i^{\text{occ}} \sum_j^{\text{unocc}} \left[\frac{\bar{\psi}_i^*(\mathbf{r})\bar{\psi}_j(\mathbf{r})\bar{\psi}_j^*(\mathbf{r}')\bar{\psi}_i(\mathbf{r}')}{\omega - \varepsilon_j + \varepsilon_i + i\delta} - \frac{\bar{\psi}_i(\mathbf{r})\bar{\psi}_j^*(\mathbf{r})\bar{\psi}_j(\mathbf{r}')\bar{\psi}_i^*(\mathbf{r}')}{\omega + \varepsilon_j - \varepsilon_i - i\delta} \right] , \tag{57}$$

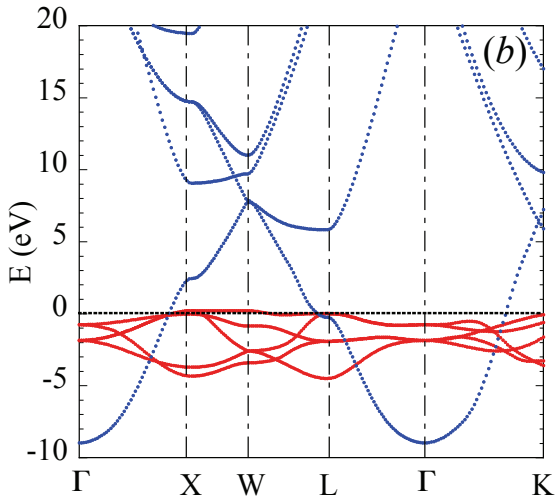

Fig. 9: *The disentangled band structure of paramagnetic nickel obtained by diagonalising the Hamiltonian in (59) taken from [25]. The red bands correspond to maximally localised Wannier orbitals of* $3d$ *character which form the* d *subspace. The blue curves correspond to the* r *subspace.*

and $P_r = P - \bar{P}_d$ can be used to calculate W_r. We found that this procedure does not work either and is again unstable for a similar reason as the one described above. Moreover, $\bar{\psi}_i$'s are not orthogonal with each other, and transitions between the states do not correspond to single particle-hole excitations.

Based on these observations we propose the following procedure [25]. We define the r subspace by

$$|\phi_i\rangle = (1 - \hat{\mathcal{P}})|\psi_i\rangle \tag{58}$$

which is orthogonal to the d subspace constructed from the Wannier orbitals. In practice it is convenient to orthonormalise $\{\phi_i\}$ and prepare $N - N_d$ basis functions. By diagonalising the Hamiltonian in this subspace a new set of wavefunctions $\{\tilde{\phi}_i\}$ and eigenvalues $\{\tilde{e}_i\}$ $(i = 1, \ldots, N - N_d)$ is obtained. Since the subspaces formed by $\{\phi_i\}$ and $\{\tilde{\psi}_j\}$ are orthogonal, the set of $(N - N_d)$ bands $\{\tilde{e}_i\}$ are completely disentangled from those of the d space $\{\tilde{\varepsilon}_j\}$, and they are slightly different from the original band structure $\{\varepsilon_i\}$. Numerical tests show that the disentangled band structure is close to the original one as may be seen in the example of nickel in Figs. 8 and 9. The form of the Hamiltonian is illustrated below

$$H = \begin{bmatrix} H_{dd} & 0 \\ 0 & H_{rr} \end{bmatrix}, \tag{59}$$

where H_{dd} is the Hamiltonian matrix taken in the d subspace $\{\tilde{\psi}_j\}$ and H_{rr} is taken in the subspace of $\{\phi_i\}$. In other words, the coupling between the d and r subspaces is set to zero.

The Hubbard U is then calculated according to Eq. (44) with $P_r = \tilde{P} - \tilde{P}_d$, where $\tilde{P}$ is the full polarisation calculated for the *disentangled* band structure. We note that the screening processes between the d and r subspaces are not neglected but included in P_r, although the d-r coupling is

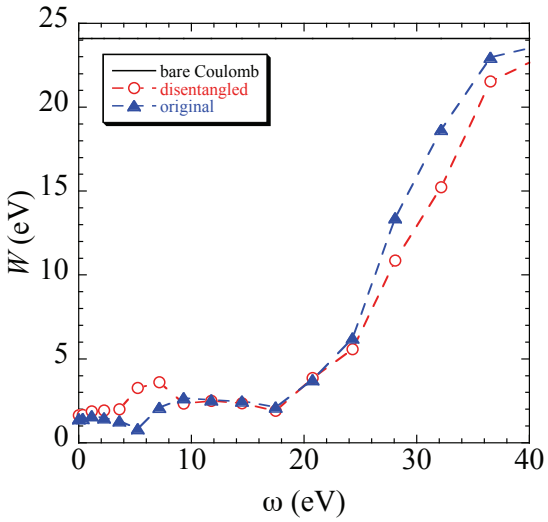

Fig. 10: *Comparison between the fully screened interactions W of nickel for the normal case with the original band structure (triangle, blue) and for the case where the band structure is disentangled (circle, red).*

cut off in the construction of the wavefunctions and eigenvalues. In the Appendix, the flowchart for the calculation of the Hubbard U is shown.

3.6 Examples: Ni and Ce

3.6.1 Nickel

As applications of the cRPA method for entangled bands, we have calculated the Hubbard U for the $3d$ transition metal series. In Fig. 10 we compare for the case of nickel the fully screened interaction W calculated using the disentangled $3d$ bands with W calculated using the original band structure. The agreement between the two are quite satisfactory for our purpose. Most of the error arising from the disentanglement originates from regions in k-space where the $3d$ bands and the 4s-4p bands hybridise and repel each other. After the disentanglement, these bands cross rather than repel each other, as can be seen by comparing Figs. 8 and 9.
The resulting frequency-dependent Hubbard U and the exchange J for nickel are shown in Figs. 11 and 12, respectively. The complete removal of low-energy excitations within the d subspace when calculating P_r ensures that U has little structure at low energy within the band width of the d subspace. The only remaining low-energy transitions come mainly from the $4s$ band. The increase in U at around 20 eV is due to the coupling to plasmon excitations, which in the case of transition metals form a rather broad excitation.
J has a relatively weak dependence on energy, and its static value is approximately given by the unscreened value although some screening effects reducing the unscreened value from 0.8 eV to 0.7 eV at zero frequency can be observed. This is in agreement with the usual practice of taking the atomic J value, which corresponds approximately to the unscreened value, implicitly assuming that screening effects are small for the Coulomb potential arising from the exchange

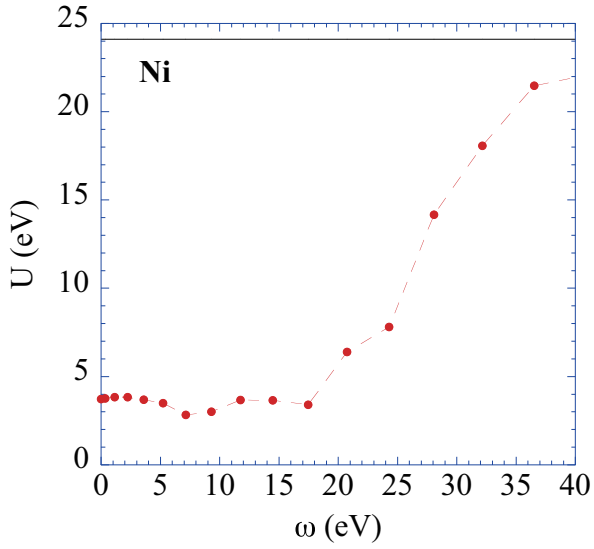

Fig. 11: *The Hubbard U of paramagnetic nickel as defined in (52) obtained using the cRPA method for disentangled bands as explained in the article. The value is averaged over the diagonal elements of the $3d$ orbitals.*

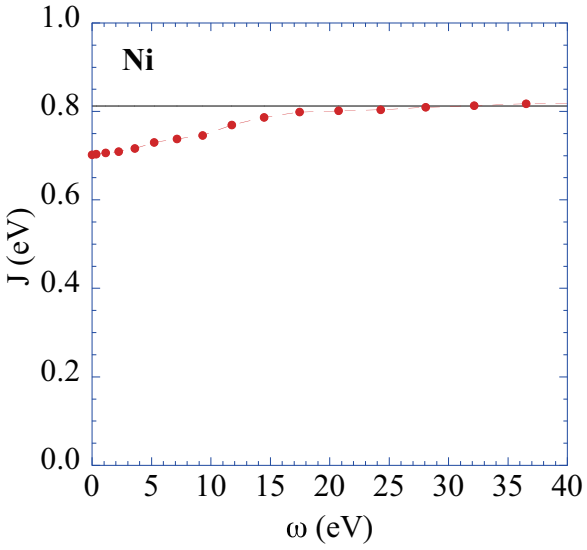

Fig. 12: *The exchange integral J as defined in (53) averaged over the $3d$ orbitals.*

charge distribution with no $l = 0$ component. In Fig. 13 the static U values for the $3d$ transition metals series are shown (red circles).

3.6.2 Cerium

As a further application, we have calculated the Hubbard U of the isostructural α and γ fcc ceriums, where the former has a smaller unit volume than the latter. As in the case of transition metals, the narrow $4f$ bands for which U is to be calculated, are entangled with the $5d$ and $6s$ bands. The Hubbard U as a function of frequency is surprisingly rich in structure with no less than five prominent peaks with smaller additional features in $\mathrm{Im}(U)$ inducing the Kramers-

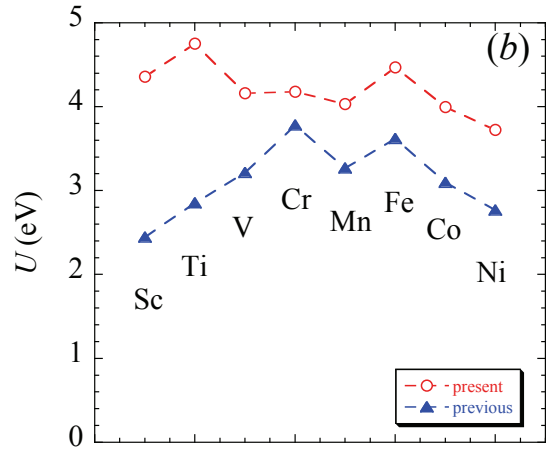

Fig. 13: *The static values of the Hubbard U for the $3d$ transition metal series taken from [25]. The results using the disentanglement method are compared with previous results, where the d subspace was defined according to a combination of band indices and energy window [23]. The significant difference between the two sets of results indicates that the Hubbard U can be sensitive to the choice of the d subspace when the bands are entangled.*

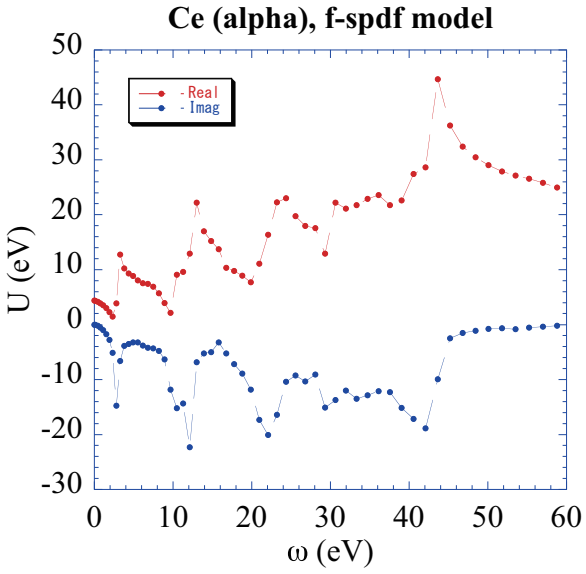

Fig. 14: *The real and imaginary parts of the Hubbard U of cerium. The d subspace is taken to be the $4f$ bands extracted using the maximally localised Wannier function method. The calculation is done using the cRPA method for entangled bands as described in the text.*

Kronig structures in $\mathrm{Re}(U)$. Unlike the usual case where there is only one prominent plasmon excitation, there appears to be several high-energy sub-plasmon excitations. The structure at low energy around 4 eV indicates that there is a large screening contribution arising from the polarisation between the d and r subspaces at low energy. It suggests that model calculations with a static U may not be sufficient for describing the electronic spectra of cerium even at low energies. Fortunately, very recently a new method to solve the impurity problem within

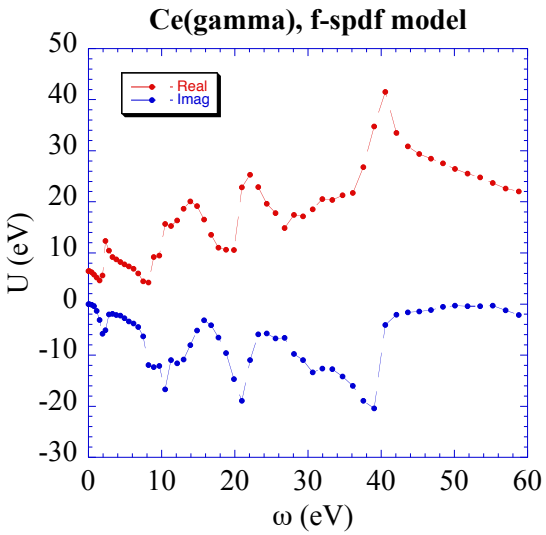

Fig. 15: *The same as Fig. 14 but for the γ phase.*

the dynamical mean-field theory (DMFT) with a frequency-dependent U has been developed [26, 27].

The subtle difference between the α and γ phases is revealed in U. The peak in $\mathrm{Im}(U)$ at low energy is larger for the α than the γ phase. This is consistent with the fact that the γ phase has a larger unit cell volume so that the $4f$ bands are narrower than in the α phase. This means that $P_r = P - P_d$ for the γ phase contains less low energy transitions between the d and r subspaces because there is less hybridisation between the $4f$ states and other states, compared with the α phase.

3.7 Further examples

The cRPA method has by now been applied to a wide range of materials from simple ones like $3d$ transition metals to complex ones such as the BEDT-TTF organic conductors [17], alkali cluster-loaded soladites [28] and the parent compounds of the recently discovered superconducting iron-based pnictides [29, 30]. In the latter reference, the U and J for a series of pnictides have been systematically calculated. It appears from this study that FeSe is more correlated compared to the other pnictides.

Other applications include calculations of the Hubbard U of MnO as a function of pressure [31]. Recently, the frequency-dependent Hubbard U of the parent cuprate superconductor La_2CuO_4 was calculated [32]. With the development of a new method it is now possible to solve the impurity problem within the DMFT method with a frequency-dependent Hubbard U [26, 27]. This method was very recently applied to study the electronic structure of $BaFe_2As_2$, one of the parent compounds of the iron-based superconducting pnictides [33].

Appendices

A Basis functions

The Bloch wavefunctions $\psi_{\mathbf{k}n}(\mathbf{r})$ are expanded in terms of the LAPW basis, i.e., in the interstitial region

$$\psi_{\mathbf{k}n}(\mathbf{r}) = \frac{1}{\sqrt{\Omega}} \sum_{\mathbf{G}} c_{\mathbf{k}n,\mathbf{G}} e^{i(\mathbf{k}+\mathbf{G})\cdot\mathbf{r}} \tag{60}$$

with the unit-cell volume Ω and inside the muffin-tin sphere of atom a

$$\psi_{\mathbf{k}n}(\mathbf{r}) = \sum_{lm} \left[A_{alm,n}(\mathbf{k}) u_{al}(r) + B_{alm,n}(\mathbf{k}) \dot{u}_{al}(r)\right] Y_{lm}(\hat{\mathbf{r}}), \tag{61}$$

where $\mathbf{r}$ is measured from the sphere centre. The coefficients $c_{\mathbf{k}n,\mathbf{G}}$, $A_{alm,n}(\mathbf{k})$, and $B_{alm,n}(\mathbf{k})$ are determined such that the wave functions and their radial derivatives are continuous at the muffin-tin sphere boundaries. The radial functions $u_{al}(r)$ and $\dot{u}_{al}(r)$ are the solution of the radial Schrödinger equation or the scalar-relativistic Dirac equation [34] and its energy derivative, respectively. Evidently for spin-polarised or relativistic systems all the above quantities depend on the spin variable.

The basis functions needed to calculate the response functions and the screened interaction or the Hubbard U are constructed as follows [19, 20]. From (38) it is clear that the space spanned by the polarisation function P is formed by products of orbitals. In terms of the LAPW basis within the muffin-tin spheres these products are

$$\left\{u_{al}u_{al'}\right\}, \left\{u_{al}\dot{u}_{al'}\right\}, \left\{\dot{u}_{al}\dot{u}_{al'}\right\} \otimes Y_{lm}Y_{l'm'}, \tag{62}$$

which form a complete basis for P and R inside the muffin-tin spheres. That the basis is also complete for R may be seen by expanding R in (32) in terms of P:

$$R = P + PvP + PvPvP + ... \tag{63}$$

Since the left and right of R are both projected onto P, the space spanned by P and R are the same. It turns out that the products in (62) can be linearly dependent since they are not orthogonal. To remove this linear dependency and to construct the optimal basis set we follow the procedure in [19, 20]. Calling the orbital products $\{b_\alpha\}$ as in (39) we calculate the overlap matrix

$$O_{\alpha\beta} = \langle b_\alpha | b_\beta \rangle, \tag{64}$$

and diagonalise it. Linear dependency is indicated by zero or very small eigenvalues. The eigenvectors of O form an orthogonal basis and by discarding those eigenvectors with eigenvalues lower than a certain tolerance, set according to desired accuracy, we obtain an optimal basis for the muffin-tin region. The basis for the interstitial part is naturally given by the plane waves, which already form a product basis since any product of two plane waves yields another plane wave.

B Flow chart

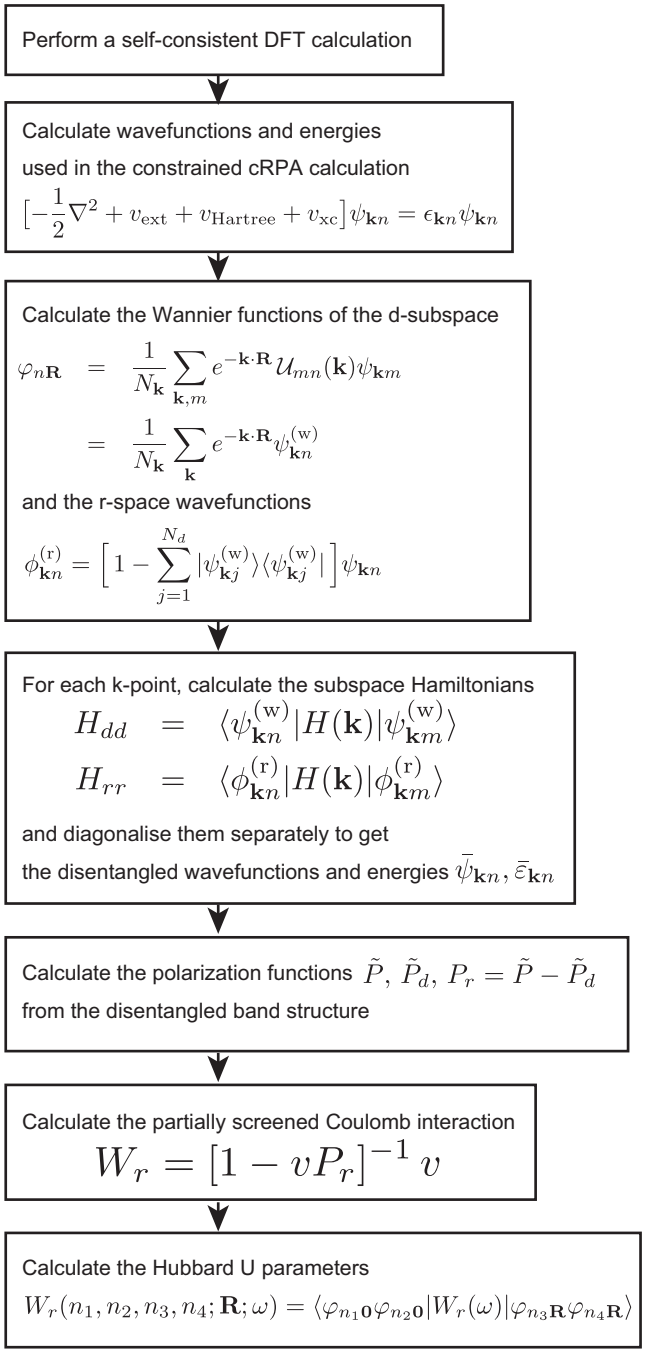
Perform a self-consistent DFT calculation
Calculate wavefunctions and energies
used in the constrained cRPA calculation
$\left[-\frac{1}{2}\nabla^2 + v_{\rm ext} + v_{\rm Hartree} + v_{\rm xc}\right]\psi_{\mathbf{k}n} = \epsilon_{\mathbf{k}n}\psi_{\mathbf{k}n}$
Calculate the Wannier functions of the d-subspace
$\varphi_{n\mathbf{R}} = \frac{1}{N_{\mathbf{k}}}\sum_{\mathbf{k},m} e^{-\mathbf{k}\cdot\mathbf{R}}\mathcal{U}_{mn}(\mathbf{k})\psi_{\mathbf{k}m}$
$= \frac{1}{N_{\mathbf{k}}}\sum_{\mathbf{k}} e^{-\mathbf{k}\cdot\mathbf{R}}\psi^{(\rm w)}_{\mathbf{k}n}$
and the r-space wavefunctions
$\phi^{(\rm r)}_{\mathbf{k}n} = \Big[1 - \sum_{j=1}^{N_d} |\psi^{(\rm w)}_{\mathbf{k}j}\rangle\langle\psi^{(\rm w)}_{\mathbf{k}j}|\Big]\psi_{\mathbf{k}n}$
For each k-point, calculate the subspace Hamiltonians
$H_{dd} = \langle\psi^{(\rm w)}_{\mathbf{k}n}|H(\mathbf{k})|\psi^{(\rm w)}_{\mathbf{k}m}\rangle$
$H_{rr} = \langle\phi^{(\rm r)}_{\mathbf{k}n}|H(\mathbf{k})|\phi^{(\rm r)}_{\mathbf{k}m}\rangle$
and diagonalise them separately to get
the disentangled wavefunctions and energies $\bar{\psi}_{\mathbf{k}n}, \bar{\varepsilon}_{\mathbf{k}n}$
Calculate the polarization functions $\tilde{P}$, $\tilde{P}_d$, $P_r = \tilde{P} - \tilde{P}_d$
from the disentangled band structure
Calculate the partially screened Coulomb interaction
$W_r = [1 - vP_r]^{-1}\, v$
Calculate the Hubbard U parameters
$W_r(n_1, n_2, n_3, n_4; \mathbf{R}; \omega) = \langle\varphi_{n_1\mathbf{0}}\varphi_{n_2\mathbf{0}}|W_r(\omega)|\varphi_{n_3\mathbf{R}}\varphi_{n_4\mathbf{R}}\rangle$

References

[1] A.L. Fetter and J.D. Walecka, *Quantum Theory of Many-Particle Systems* (Dover, New York 2003)

[2] J. Hubbard, Proc. Roy. Soc. A 276 238 (1963)

[3] M. Imada, A. Fujimori, and Y. Tokura, Rev. Mod. Phys. **70**, 1039 (1998)

[4] W.M.C. Foulkes, L. Mitas, R.J. Needs and G. Rajagopal, Rev. Mod. Phys. **73,** 33–83 (2001)

[5] A. Georges *et al.*, Rev. Mod. Phys. **68**, 13 (1996)
G. Kotliar and D. Vollhardt, *Physics Today,* 53 (March 2004)

[6] O. Gunnarsson, O.K. Andersen, O. Jepsen, and J. Zaanen, Phys. Rev. B **39**, 1708 (1989)
O. Gunnarsson, Phys. Rev. B **41**, 514 (1990)
V.I. Anisimov and O. Gunnarsson, Phys. Rev. B **43**, 7570 (1991)

[7] M.S. Hybertsen, M. Schlüter and N.E. Christensen, Phys. Rev. B **39**, 9028 (1989)

[8] A.K. McMahan, R.M. Martin and S. Satpathy, Phys. Rev. B **38**, 6650 (1988)

[9] M. Cococcioni and S. de Gironcoli, Phys. Rev. B **71**, 035105 (2005)

[10] M. Springer and F. Aryasetiawan, Phys. Rev. B **57**, 4364 (1998)

[11] T. Kotani, J. Phys: Condens. Matter **12,** 2413 (2000)

[12] N.W. Ashcroft and N.D. Mermin, *Solid State Physics* (Brookes Cole, 1976)

[13] J. Schwinger, *Proc. Natl. Acad. Sci., USA,* **37**, 452 (1951)

[14] L. Hedin, Phys. Rev. **139**, A796 (1965); L. Hedin and S. Lundqvist, *Solid State Physics* Vol. 23, eds. H. Ehrenreich, F. Seitz, and D. Turnbull (Academic, New York, 1969)

[15] F. Aryasetiawan *et al*, Phys. Rev. B **70**, 195104 (2004)

[16] F. Aryasetiawan, J. Tomczak, T. Miyake, and R. Sakuma, Phys. Rev. Lett. **102**, 176402 (2009)

[17] K. Nakamura, Y. Yoshimoto, T. Kosugi, R. Arita, and M. Imada, J. Phys. Soc. Jap. **78**, 083710 (2009)

[18] O.K. Andersen, Phys. Rev. B **12**, 3060 (1975)

[19] F. Aryasetiawan and O. Gunnarsson, Phys. Rev. B **49**, 16214 (1994)

[20] F. Aryasetiawan and O. Gunnarsson, Rep. Prog. Phys. **61**, 237 (1998)

[21] N. Marzari and D. Vanderbilt, Phys. Rev. B **56**, 12847 (1997)
I. Souza, N. Marzari and D. Vanderbilt, Phys. Rev. B **65**, 035109 (2001)

[22] T. Miyake and F. Aryasetiawan, Phys. Rev. B **77**, 085122 (2008)

[23] F. Aryasetiawan, K. Karlsson, O. Jepsen, and U. Schönberger, Phys. Rev. B **74**, 125106 (2006)

[24] O.K. Andersen and T. Saha-Dasgupta, Phys. Rev. B **62**, R16219 (2000)
F. Lechermann *et al.*, Phys. Rev. B **74**, 125120 (2006)

[25] T. Miyake, F. Aryasetiawan, and M. Imada, Phys. Rev. B **80**, 155134 (2009)

[26] P. Werner and A.J. Millis, Phys. Rev. Lett. **99**, 146404 (2007)

[27] P. Werner and A.J. Millis, Phys. Rev. Lett. **104**, 146401 (2010)

[28] K. Nakamura, T. Koretsune, and R. Arita, Phys. Rev. B **80**, 174420 (2009)

[29] K. Nakamura, R. Arita and M. Imada, J. Phys. Soc. Jap. **77**, 093711 (2008)

[30] T. Miyake, K. Nakamura, R. Arita, and M. Imada, J. Phys. Soc. Jap. **79**, 044705 (2010)

[31] J. Tomczak, T. Miyake, and F. Aryasetiawan, Phys. Rev. B **81**, 115116 (2010)

[32] A.V. Kozhevnikov, A.G. Eguiluz, and T.C. Schultess, http://www.computer.org/portal/web/sc10

[33] P. Werner, M. Casula, T. Miyake, F. Aryasetiawan, A.J. Millis, and S. Biermann, http://arxiv.org/abs/1107.3128

[34] D.D. Koelling and B.N. Harmon, J. Phys. C **10**, 3107 (1977)